Landslide susceptibility analysis using event-based landslide inventories

Chih Ming Tseng[1*], Ching Weei Lin[2], Wen Don Hsieh[2]

[1]Department of Land Management and Development
Chang Jung Christian University, No. 1, Changda Road
Gueiren District, Tainan City, Taiwan (R.O.C.)

[2]Department of Earth Sciences
National Cheng Kung University, No.1, University Road
Tainan City, Taiwan (R.O.C.)

Revised paper

Submitted to Natural Hazards and Earth System Sciences

April 2015

Pages: 31

* Corresponding author

Tel: +886 6 2785123 ext.2320, Fax: +886 6 2785902

e-mail address: cmtseng@mail.cjcu.edu.tw (Tseng C.M.)

Landslide susceptibility analysis using event-based landslide inventories

Chih Ming Tseng · Ching Weei Lin · Wen Don Hsieh

Abstract This study uses landslide inventory of a single typhoon event and Weight of Evidence (WOE) analysis to prepare landslide susceptibility map of the Laonung River in southern Taiwan. Eight factors including lithology, elevation, slope, slope aspect, landform, Normalized Difference Vegetation Index (NDVI), distance to geological structure, and distance to stream are used to evaluate the susceptibility of landslide. Effect analysis and the assessment of grouped factors showed that lithology, slope, elevation, and NDVI are the factors that mostly influence the instability of the study area. Landslide susceptibility analysis with these four factors achieves over 90% of the AUC (area under curve) that represent the respective success rates and prediction rates of all eight factors. Four landslide susceptibility models for four typhoons from 2007 to 2009 are developed, and each model is cross validated. Results indicate that the best model should be developed by using landslide inventory close to the landslide occurrence threshold and should reflect the most common spatial rainfall pattern in the study region for ideal simulation and validation results. The prediction accuracy of the best model in this study reached 90.2%. The two highest susceptibility categories (very high and high levels) cover around 80% of the actual landslides in the study area.

Keywords Landslides · Weight of evidence analysis · Susceptibility map · Taiwan

1 Introduction

Landslides are a natural process that plays a key role in landscape evolution of mountainous and hilly environments. They also represent a serious hazard in many areas of the world (Brabb and Harrod 1989; Cendrero and Dramis 1996; Glade et al. 2005). In mountainous areas of Taiwan, where is located at convergent plate boundary and the annual rainfall is over 2500 mm, landslides and debris flows are major natural hazards that threaten human lives (Lin et al. 2013; Tseng et al., 2013). For example, Typhoon Morakot in August of 2009, with a maximum precipitation of over 2884 mm in 5 days, triggered over 22705 landslides, covering a total area of 274 km^2 in mountainous regions throughout southern Taiwan, with some landslides covering areas of over 60 ha (Lin et al. 2011). One deep-seated landslide, the Hsiaolin landslide, covering an area of about 250 ha, buried the entire village of Hsiaolin in Kaohsiung County, resulting in 397 casualties, 53 people missing, and the destruction of over 100 houses (Lin et al. 2011; Tsou et al. 2011). To prevent such disasters, it is essential to map the areas that are susceptible to landslide for sustainable land-use management.

Landslide susceptibility can be defined as the probability of the occurrence of a landslide based on the relationship between the occurrence distribution and a set of predisposing factors, i.e. geo-environmental thematic variables in the area (Brabb 1984; Guzzetti et al. 2005). Landslide susceptibility mapping involves handling, processing and interpreting a large amount of geographical data. Many studies have addressed landslide susceptibility mapping by various methods. Apart from the subjectivity of a direct (heuristic) approach completely based on field observations and an expert's priori knowledge, the remaining methods developed to detect the areas prone to landslide can be divided mainly into two categories: deterministic approach and statistical approach. The deterministic approach is based on the physical laws driving landslides and generally more applicable when the underground conditions are relatively homogeneous. The statistical approach is based on the relationships between the affecting factors and past and present landslide distribution (Van Westen et al. 2008). Statistical methods analyze the relation between all the factors affecting the landslide and are mainly focused on numerical methods such as linear or logistic regression (LR), artificial neural networks (ANN), frequency ratio (FR), and weight of evidence (WOE). In addition, landslide susceptibility assessment also involves the comparison of different statistical models (e.g., Lee and Pradhan 2007; Akgun et al. 2008; Yilmaz 2009; 2010a,b; Poudyal et al. 2010; Akgun 2011;

Pradhan and Lee 2010a,c; Pradhan 2011; Yalcin et al. 2011; Bui et al. 2012; Mohammady et al. 2012; Schicker and Moon 2012; Xu et al. 2012; Ozdemir and Altural 2013; Althuwaynee et al. 2014; Shahabi et al. 2014). To map the susceptibility to landslides, the WOE method calculates the weight for each factor affecting the landslide based on the presence or absence of landslides within the study area (Van Westen et al. 2003; Lee and Choi 2004; Kanungo et al. 2006; Mathew et al. 2007; Neuhäuser and Terhorst 2007; Dahal et al. 2008a,b; Barbieri and Cambuli 2009; Nandi and Shakoor 2009; Regmi et al. 2010; Ozdemir 2011; Mohammady et al. 2012; Schicker and Moon 2012; Ozdemir and Altural 2013). Conditional probability analysis is also a valuable tool in hazard zonation (Carrara et al. 2001), particularly when a few but relevant factors are available (Neuhäuser and Terhorst 2007).

In the past, because of difficulties in obtaining detailed landslide data for each rainfall event, statistics-based landslide susceptibility evaluation models were based mainly on a long-term historical inventory of landslides induced by various rainfall events or earthquakes. Now, with highly developed remote sensing technology, multi-temporal satellite or aerial images have become an efficient way to map landslides after each event. Event-based multi-temporal landslide inventories are helpful for the understanding of recurrent landslide sites, and landslide occurrence criteria reflect the rainfall scale of storms and typhoons. Thus, the adoption of an event-based landslide inventory is beneficial in establishing an optimal landslide susceptibility evaluation model. To date, there is no comprehensive study involving the application of a single event-based landslide inventory to develop and validate a landslide susceptibility model. Lee et al. (2008) used an event-based landslide inventory to evaluate landslide susceptibility; however, only one typhoon event was used to establish the susceptibility model, and the suitability of the scale of the typhoon event adopted to establish the susceptibility model was not demonstrated. The present study evaluates susceptibility to landslides through a single typhoon landslide inventory using Bayes' theorem (Papoulis 1984) based on the WOE method. We apply multi-temporal FORMOSAT-2 images to map four different rainfall scales of typhoon event-based landslide inventories. To establish an optimal model we perform cross testing of four event-based landslide inventories, i.e. one model is calibrated based on one typhoon landslide inventory and validated by the other three typhoon landslide inventories. The area under curve (AUC) of the success rate curve (training sets) and the prediction rate curve (validation sets), respectively, are applied to demonstrate the

training and predictive performance of the susceptibility values obtained by the application of WOE (Van Westen et al. 2003; Poli and Sterlacchini 2007). The dominant combination of factors related to landslide occurrence, and the most suitable rainfall scale to develop an optimal model are also discussed.

2 Study area

The Laonong River watershed of southern Taiwan with a total area of 1367 km^2 was selected as our study area (Fig. 1). The physiography is composed mainly by a series of approximately N–S to NE–SW trending mountain ranges. The elevation decreases westward and southward, from an elevation of 3941 m a.s.l. at the crest of Jade Mountain to 55 m a.s.l. at the foot of the mountain. The main river, the Laonong River, flows SW and is one of the main tributaries of the Kaoping River.

For the convenience of discussion, the exposed rocks in the study area are roughly grouped according to their age and mechanical behavior into five stratigraphic units: slate, sandstone-shale, meta-sandstone, conglomerate and gravel, and sand (Fig. 1). In which the category of gravel and sand mainly reflect the alluvial deposition in riverbed. The slope-angle distribution calculated from a 5-m grid digital elevation model (DEM) falls in the range of 20–50° (78% of the study area). The climate is a typical sub-tropical climate with a mean annual rainfall of about 2500 mm. Precipitation occurs mainly from May to September.

3 Materials and Method

3.1 Event-based landslide inventories

Four typhoons (Table 1) that occurred in 2007–2009 and induced landslides were considered in the present study to prepare the landslide susceptibility map. Landslides of each typhoon in the study area were mapped from multi-spectral FORMOSAT-2 satellite images with 8-m pixel resolution taken before and after each typhoon event (Table 1). FORMOSAT-2 satellite images have been widely applied in identification of natural disasters (e.g., Lin et al. 2004; Lin et al. 2006; Liu et al. 2007; Lin et al. 2011). Mapping of the various types of landslides induced by each typhoon included landslides that are an extension of pre-existing landslides, as well as newly formed landslides.

On a FORMOSAT-2 multi-spectral image, shallow debris slides are the easiest type of

slides to reliably detect because they strip off the vegetation cover and are thus readily discernable (Lin et al. 2011). Therefore, in this study we used mainly shallow debris slides. A landslide classification program based on Normalized Difference Vegetation Index (NDVI) (Eidenshink 1992) distribution was used to identify bare land in images of the study area. Bare land in flat areas such as river beds was ruled out automatically by using a filter that deletes areas with a slope gradient less than 10°. Bare land caused by agriculture or urban development was excluded manually, leaving the landslide-induced bare land for the analysis. To prevent misinterpretation, only landslides with a projected area over nine pixels (representing areas larger than 576 m^2) were recognized. However, cases where the vegetation was stripped off due to deep-seated slides and lateral erosion along the gully bed caused by debris flows were also included. All the mapped landslides in each typhoon event were transformed from vector format to raster format with 8-m pixel resolution. The mapped landslide inventories of four typhoons are shown in Fig. 2 and the landslide areas are summarized in Table 2, in which the landslide ratio is calculated as the total area of landslides per square km of the study area. The accumulated rainfall map of four typhoons are shown in Fig. 3 and rainfall statistics of each typhoon listed in Table 2. The rainfall data was obtained from the 1.3 km x 1.3 km mesh type QPESUMS (Quantitative Precipitation Estimation and Segregation Using Multiple Sensors) precipitation products of the Central Weather Bureau in Taiwan. The average accumulated rainfall of Typhoon Morakot reached to 2,323 mm, thus caused severe landslides in the study area. Four typhoons showed significant spatially variation in rainfall pattern. Rainfall center usually accompanies with more landslides, however in Typhoon Mitag, part area only with accumulated rainfall around 100 mm still trigger landslides. This is probably because one another Typhoon Krosa (4-7 Oct 2007) affected the study area one month ahead of Typhoon Mitag. Typhoon Krosa brought the average and maximum accumulated rainfall 585 mm and 918 mm, respectively. The critical threshold of landslide occurrence in Typhoon Mitag could possibly become lower due to the high water content of soil affected by the Typhoon Krosa.

3.2 Affecting factors related to landslides

The geo-environmental characteristics of an area affect the occurrence of landslides in different ways, and can be applied as affecting factors in the prediction of future landslides (Van Westen et al. 2008). The selection of affecting factors depends on the scale of the

132 analysis, the characteristics of the study area, the landslide type, etc. (Glade et al. 2005).
133 Nevertheless, there are no general guidelines for selecting these factors (Ayalew et al. 2005;
134 Yalcin 2008). In the present study, the affecting factors were selected among those most
135 commonly used in the literature to evaluate landslide susceptibility; in particular, the
136 results of field surveys and remote-sensing image interpretation suggest that the following
137 eight parameters: geology (lithology), geomorphology (elevation, slope, aspect and
138 landform), vegetation index, distance to geological structure, and distance to stream. To
139 prepare the landslide susceptibility model, the geomorphic parameters were directly
140 extracted from a digital elevation model (DEM) with a resolution of 5-m pixel size
141 provided by the Ministry of Interior of Taiwan. These affecting factors are assumed
142 constant over time except the vegetation index, which is extracted from the FORMOSAT-2
143 image taken before each typhoon event. The relation between the affecting factors and the
144 landslides induced by the four typhoons is shown in Fig. 4, in which the landslide ratio was
145 calculated as a ratio in percentage between the landslide area and the total area in each
146 affecting factor class. The distribution of landslide ratios shows the relative importance of
147 the different classes of affecting parameters to the landslide. Any area with a slope smaller
148 than 5° and located in the main channel is treated as a stable area of the landslide and these
149 cells are excluded in the categorization of the affecting factors.
150 Lithology is considered one of the main factors affecting landslide occurrence. By
151 integrating the 1:50,000 geological map published by the Central Geology Survey of
152 Taiwan, the lithologies in the study area are classified in five lithological groups as shown
153 in Fig. 1. The relation between the lithology and landslide inventories of the four typhoons
154 shows that landslides occurred mainly in sandstone-shale and slate.
155 Elevation is a factor frequently utilized in landslide susceptibility assessment. The
156 elevation in the study area varies from 55 to 3941 m; it was divided into thirteen heights at
157 intervals of 250 m (Yalcin 2008; Regmi et al. 2010; Tang et al. 2011). The relation
158 between landslide distribution and elevation (Fig. 4) shows a significant variation among
159 the four typhoons. In Typhoons Mitag, Sinlaku and Morakot, the elevation factor generally
160 varies inversely to the landslide ratio while Typhoon Kalmagei shows an opposite trend.
161 This is most likely due to the spatial variation of typhoon rainfall.
162 In previous studies of landslide susceptibility, slope was also considered as major
163 factor affecting slope stability (Anbalagan 1992; Pachauri et al. 1998; Saha et al. 2002;
164 Yalcin 2008) because the driving force of mass movement increases with increasing slope

(Guillard and Zezere 2012). The slopes in the study area were divided into seven classes with an interval of 10° (Van Westen et al. 2003, Dahal et al. 2008a,b, Regmi et al. 2010). The relation between landslides and slope angle (Fig. 4) shows that most of the landslides were observed for slopes >30°. In Typhoon Morakot, many landslides occurred at slopes of 21–30° (nearly 6.7% of the landslide ratio).

The aspect of the slope plays a role in controlling some microclimatic factors such as exposure to sunlight and windward (wet) or leeward (dry) conditions, rainfall intensity, soil moisture, and weathering, all of which control the material properties of the slope deposits (Dai et al. 2001; Cevik and Topal 2003). The aspect of the study area was classified into eight classes (N, NE, E, SE, S, SW, W, and NW) with the addition of flat areas. Apart from the flat area, south-facing and SW-facing aspects dominate the aspect classes of the study area. The relation between aspect and landslide occurrences (Fig. 4) shows a similar trend for Typhoons Mitag, Sinlaku, and Morakot, where most of the landslides were observed in areas with south-facing slopes (SW, S, SE). However, for Typhoon Kalmagei areas with north-facing slopes were dominant, probably due to the typhoon path that induced spatial variation in the rainfall.

Landform plays an important role in contributing to terrain instability, and can usually be analyzed by combing different types of curvatures such as plan curvature and profile curvature. The term curvature is theoretically defined as the rate of change of the slope gradient or aspect, usually in a particular direction (Wilson and Gallant 2000). The curvature value can be evaluated by calculating the reciprocal value of the radius of the curvature in a particular direction and obtained directly from the derivatives of the topographical surface (Wilson and Gallant 2000). The landform of the study area was classified into nine classes based on the method proposed by Dikau (1989). Considering the cross combination of convex, straight, concave type in profile curvature and ridge, slope, valley type in plain curvature, then nine classes are obtained. The relation between the landslide occurrence and landform (Fig. 4) shows that more landslides appeared in the concave or valley landforms.

The vegetation index is also considered an influencing factor in landslide susceptibility assessment studies (Althuwaynee et al. 2012). NDVI was used in this study to reflect the vegetation density. In general, the value of NDVI ranged from −1 to 1; the higher the value of NDVI the denser of vegetation cover. The NDVI value was calculated by using the multi-spectrum information from the FORMOSAT-2 image based on the

following formula.

$$\mathrm{NDVI} = \frac{\mathrm{NIR} - \mathrm{R}}{\mathrm{NIR} + \mathrm{R}} \quad (1)$$

where NIR is the reflectance in the near-infrared wave band and R is the reflectance in the red wave band. The NDVI value in our study area was less than 0.8; therefore the NDVI was classified into four levels between 0–0.8 with a 0.2 interval, and a fifth level which included NDVI values less than 0. The relation between landslide occurrence and NDVI (Fig. 4) shows that most of the landslides were in areas with low NDVI values, especially NDVI < 0.

Geological structures such as faults and folds usually play an important role in landslide formation. High susceptibility to landslides has been widely recorded at sites close to geological structure which not only affects the surface landform but also contributes to soil permeability causing slope failure. The distance between the landslide and the geological structure in the study area was classified into ten lengths from 200 m to 2000 m, at 200 m steps, with an additional eleventh category for distances greater than 2000 m (Lee and Choi 2004; Vijith and Madhu 2008). The relation between landslide occurrences and distance to geological structure (Fig. 4) shows that a little higher landslide ratio were observed in the area with a distance to geological structure ranging from 1400–2000 m.

The network of rivers and streams is another controlling parameter of landslide occurrence, as stream erosion may undercut the foot of the slopes as well as saturate their lower part (Dai et al. 2001; Saha et al. 2002; Cevik and Topal 2003; Yalcin 2008). The stream network was extracted by using the HYDRO tools of the ArcGIS software from the 5-m resolution DEM. The distance to the stream was then classified into nine lengths from 50 m to 450 m, at 50 m steps with an additional tenth category for distances greater than 450 m. The ‘distance to stream’ factor shows a significant inverse relation with landslide occurrences, the closer the site was to the stream, the more landslides were observed.

3.3 Weight of evidence

Weight-of-evidence (WOE) is one of the bivariate methods first applied to mineral exploration (Bonham-Carter et al. 1988). Subsequently, Van Westen et al. (2003) utilized the method for landslide susceptibility assessment. The theoretical background and its

application in landslide susceptibility assessment are presented in many studies (see Introduction). The model is based on a log-linear form of Bayes' theorem, which calculates the weight for each affecting factor based on the combinational probabilities of its presence or absence with the presence or absence of a landslide within each map unit area (Bonham-Carter 2002). The WOE method was documented mathematically by Van Westen et al. (2003) and Regmi et al. (2010) in detail. We calculated the weighted values for the classes of affecting factors related to landslides by using the following equations (Regmi et al. 2010):

$$W^{+} = \ln\left(\frac{\frac{A_1}{A_1 + A_2}}{\frac{A_3}{A_3 + A_4}}\right) \quad (2)$$

$$W^{-} = \ln\left(\frac{\frac{A_2}{A_1 + A_2}}{\frac{A_4}{A_3 + A_4}}\right) \quad (3)$$

where A_1 is the number of landslide meshes present in a given factor class, A_2 is the number of landslide meshes not present in the given factor class, A_3 is the number of meshes in the given factor class in which no landslide meshes are present, and A_4 is the number of the meshes in which neither landslides nor the given factor are present. A positive weight (W^{+}) indicates the presence of the affecting factor in the landslide, and the magnitude of this weight is an indication of the positive correlation between the presence of the affecting factor and landslides. A negative weight (W^{-}) indicates an absence of the affecting factor, and its magnitude indicates negative correlation (Regmi et al. 2010). The difference between Eq. (2) and Eq. (3) is defined as the weight contrast, C ($C = W^{+} - W^{-}$). A weight value of C = 0 indicates that the considered class of the affecting factor is not significant for the analysis. Positive or negative contrast indicates a positive or negative spatial correlation, respectively (Piacentini et al. 2012). The final landslide susceptibility index LSI is calculated by combining the probabilities associated with the different components of the model (Barbieri and Cambuli 2009):

$$LSI = \exp\left(\sum W^{+} + \ln(O_f)\right) \quad (4)$$

where $O_f = P_f/(1-P_f)$ is the prior odds of a landslide in the study area, and $P_f = A_f / A_t$ where

A_f is the portion of the study area affected by landslides and A_t is the total study area (Shicker and Moon 2012).

4 Results and discussion

4.1 Testing for the predominant factors of landslides

The factors related to the occurrence of landslides are usually selected in the landslide susceptibility analysis. It is, however, worth discussing whether all the selected factors are required in the analysis. Previous studies have used effect analysis to identify factors or groups of factors that significantly influence landslide prediction (Van Westen et al. 2003; Dahal et al. 2008a,b). To do so, the factors are grouped directly, or in some cases certain factors are excluded before the weights are added. The predicted result is then compared to that obtained using all of the factors. Any obvious changes observed in the comparison would indicate the excluded or selected factors' significant impact on the prediction of landslides (Lee and Talib 2005). In previous studies, effect analysis was mostly conducted by eliminating some of the factors or selecting certain factor combinations in order to observe the unselected factors and their effects on the results (Van Westen et al. 2003; Lee and Talib 2005; Dahal et al. 2008a,b).

This study adopts an unconventional approach for the analysis. First, we select lithology and slope, the two most frequently used factors in previous studies, to be the primary factor combination for testing and analysis. Then, we enter additional factors and observe after each addition the changes to the AUC of the success rate curve. The process repeats itself and the factors are gradually accumulated until no more obvious changes in the AUC can be observed. The final test combination consists of eight factors. These factors were identified as the predominant factors of the landslides, having significant influences on the AUC of the success rate curve. Table 3 shows the test results for the predominant factor combinations of the typhoon events in the study. As the number of factors tested increases, the AUC also shows an increase. This highlights the increasing explanatory power of the factors. Using only four to five of the total eight factors for training, each typhoon event produces an AUC result similar to that of all eight factors, with a difference of less than 0.03. For example, the factor combination of lithology, slope, and NDVI reaches 90% of the AUC of all the factors combined for Typhoons Sinlaku, Mitag, and Kalmaegi; the combination of lithology, slope, and elevation reaches 90% of the AUC for Typhoon Morakot. Therefore, lithology, slope, elevation, and ground

vegetation are the predominant factors affecting a large number of landslides in the whole area. As for the other factors, aspect is affected by the spatial variation of the rainfall during the typhoon or monsoon (i.e. whether the slope is facing windward or leeward).

From the perspective of statistics, effect analysis can indeed simplify the factor selection in the susceptibility analysis. In previous studies, effect analysis was conducted primarily in two ways: (1) a factor is excluded and the influence of the excluded factor on the result is assessed (Lee and Talib 2005) and (2) factors are divided into categories of lithology, topography, and human cause; then, the categories are analyzed to assess the selected factors' influences on the results (Van Westen et al. 2003; Dahal et al. 2008a,b). The first method can identify the level of influence each factor has on the results, but it is only of statistical significance. Evaluating a factor as having a low level of influence does not mean it is not important in the susceptibility analysis (Lee and Talib 2005) need more explanation. In addition, this method cannot find the optimum factor combination. The second method grouped factors based on lithology; however, the method cannot simplify factors effectively as it may overlook important ones in different categories. In our analysis we first select the fundamental factors of landslide according to the lithology of the study region. Then, we gradually increase the number of factors in the process of effect analysis. Our results show that although this method is more time-consuming compared to the previous two methods, it effectively simplifies the landslide factors without overlooking the important ones in the analysis process.

4.2 Landslide susceptibility mapping and validation

In this study, each of the four landslide susceptibility models is prepared based on an event-based landslide inventory of a single typhoon. The landslide inventories of three other typhoon events are used to validate the landslide susceptibility prediction. Table 4 and Fig. 5 show the cross validation results of the events. Among the four typhoon events, Sinlaku exhibits the most favorable performance in developing a susceptibility model, with the success rate of the curve’s AUC reaching 0.933, followed by Mitag and Kalmaegi, with AUCs of 0.888 and 0.824, respectively. All three events show AUCs of over 80%. The AUC of Morakot is 0.657, showing a less satisfactory performance. Table 4 shows a positive correlation between the validation result and the performance in developing a susceptibility model. A higher AUC indicates a more favorable validation result. Generally among the four typhoons, the performance in developing a susceptibility model and the

validation result are directly proportional to the scale of the landsides caused by the typhoons. Better prediction results can be obtained by using the landslide susceptibility model developed based on landslide inventories triggered by the rainfall amount close to the critical threshold for landslide to occur (e.g. Sinlaku). The susceptibility model developed with the Typhoon Sinlaku event, for example, rendered satisfactory validation results in both Mitag and Kalmaegi. Mitag, in particular, showed the most favorable result, in which the AUC of the prediction rate curve reached 0.902. The model developed based on Mitag also rendered an AUC of 0.889 in Sinlaku. The validation result of the model established based on Kalmaegi (with a new landslide rate of 1.062%), on the other hand, only worked favorably for Mitag (0.712). As for Morakot, the performances for both the model and the validation were unsatisfactory. Thus, median scale rainfall induced landslides tend to render better model performances because the relative weight between the landslide factors and landslide occurrence obtained using WOE often better reflects the critical threshold for the landslides. Morakot, the largest of the four typhoons, is the most severe typhoon that impact Taiwan in the past fifty years. The QPESUM data show a mean accumulated rainfall of 2,323 mm in the study area (see Table 2). Rainfall of such scale far exceeds the critical rainfall threshold required for landslides to occur. As such, excessive landslides happened in the study area. In other words, when the landslide inventory of such a large-scale event is used to develop a model, the weight distribution among the landslide factors and landslide occurrence does not effectively distinguish areas that are susceptible to landslides from those that are not. Therefore, an inventory of a large-scale landslide fails to accomplish the optimal performance in establishing a susceptibility model. By the same token, Morakot does not help identify the threshold of landslide occurrence because of the extensive landslide area. As a result, the validation result for Morakot is unfavorable.

Mitag and Kalmaegi show similar performances in developing the susceptibility models; however, Mitag's validation result is clearly better than that of Kalmaegi. This is most likely caused by the slope aspect factor. The distribution of landslide ratios on the respective aspects for Kalmaegi is different from those of the other three typhoons (Fig. 4). Landslides that occurred during Mitag, Sinlaku, and Morakot show an obvious distribution on the south-facing aspects (SW, S, SE), while landslides caused by Kalmaegi concentrate around the north-facing aspects (NW, N, NE). As such, the distribution of weight contrast for Kalmaegi in terms of the aspects is opposite to those of the other three typhoons during the model training (Fig. 6). The northeast side of the study region is of a higher topography

that gradually descends toward the southwest. Typhoons that rotate counterclockwise cause a greater number of landslides on the southern slope because it is the windward slope where rainfall is heavier, and this is true for Mitag, Sinlaku, and Morakot (Fig. 4). Despite the satisfactory training result of Kalmaegi, the validation result is unfavorable when we use different aspect factors from other events, as they affect the weights differently. Based on the above, we see that when a landslide susceptibility model is developed based on a new landslide inventory of a single event, the selected inventory should be of a scale that is close to the landslide occurrence threshold and should reflect the most common spatial rainfall pattern in the study area for relatively ideal training and validation results.

Finally, based on the landslide inventory of Typhoon Sinlaku, which shows the best training and validation results, we prepared the landslide susceptibility map shown in Fig. 7. The susceptibility scale is based on the values of the horizontal axes of the prediction rate curves, with 0–0.1 = very high, 0.1–0.3 = high, 0.3–0.5 = moderate, 0.5–0.7 = low, and 0.7–1 = very low (Dahal et al. 2008a). The landslide ratios for each of the typhoons in the five susceptibility levels are listed in Table 5. Excluding Sinlaku, which was used to establish the susceptibility model and the extreme event of Morakot, over 80% of the actual landslide area of the other two typhoons is covered by areas of very high and high susceptibility levels. For Mitag, 92.45% of landslides occurred within the predicted landslide area, while 83.15% of the Kalmaegi landslides were within the predicted range, indicating favorable prediction results of the landslide susceptibility map based on the landslide inventory of Typhoon Sinlaku.

Previous studies that used WOE method to evaluate landslide susceptibility indicate that the prediction accuracy is in a slightly negative correlation with the area of the study region (Table 6). The larger the area, the greater the spatial difference among the topographic factors. This has an effect on the various types of landslides that occur. As a result, the training and validation results of landslide susceptibility models covering larger areas show unsatisfactory performances. Our study area spanned 1,367 km^2, which is large compared with those in other relevant studies. The prediction accuracy of the landslide susceptibility map in this study reached 90.2% in the best scenario. This supports the advantage of using a landslide inventory of a single event to develop the landslide susceptibility model to predict landslide occurrence.

5 Conclusions

By using WOE method, this study adopted a single typhoon event-based landslide inventory to develop a landslide susceptibility model. Grouping test of eight factors indicates lithology, slope, elevation, and ground vegetation are the dominant factors affecting most landslide incidents in the study area. These four factors can help achieve 90% of the AUC of the all-factor success rate curve. Cross validation of four susceptibility models show that using landslide inventories triggered by a rainfall amount close to the critical condition of landslides to develop the susceptibility models leads to more favorable landslide prediction results. This is because the relative weight between the landslide factors and landslide occurrences in the WOE analysis can often better reflect the threshold for landslides to occur. Among the four typhoon events, Typhoon Sinlaku, which demonstrated the best training and validation results, was selected to prepare the landslide susceptibility map. More than 80% of the actual landslides resulting from Typhoons Mitag and Kalmaegi are covered in the susceptibility map by areas denoted as having very high and high susceptibility to landslides. According to the results of this study, when a new landslide inventory of a single event is used to create a landslide susceptibility model, the inventory selected should be of a scale that is close to the landslide occurrence threshold, and is able to reflect the most common spatial rainfall pattern in the study area for best prediction results.

References

Akgun A, Dag S, Bulut F (2008) Landslide susceptibility mapping for a landslideprone area (Findikli, NE of Turkey) by likelihood frequency ratio and weighted linear combination models. Environmental Geology 54(6):1127–1143

Akgun A (2011) A comparison of landslide susceptibility maps produced by logistic regression, multi-criteria decision, and likelihood ratio methods: a case study at İzmir, Turkey. Landslides 9(1):93-106

Althuwaynee OF, Pradhan B, Lee S (2012) Application of an evidential belief function model in landslide susceptibility mapping. Computers & Geosciences 44:120–135

Althuwaynee OF, Pradhan B, Park HJ, Lee JH (2014) A novel ensemble bivariate statistical evidential belief function with knowledge-based analytical hierarchy process and multivariate statistical logistic regression for landslide susceptibility mapping. Catena 114:21-36

Anbalagan D (1992) Landslide hazard evaluation and zonation mapping in mountainous terrain. Engineering Geology 32:269–277

Ayalew L, Yamagishi H, Marui H, Kanno T (2005) Landslides in Sado Island of Japan Part II. GIS-based susceptibility mapping with comparisons of results from two methods and verifications. Engineering Geology 81:432–445

Barbieri G, Cambuli P (2009) The weight of evidence statistical method in landslide susceptibility mapping of the Rio Pardu Valley (Sardinia, Italy). 18th World IMACS/MODSIM Congress, Cairns, Australia.

Bonham-Carter GF, Agterberg FP, Wright DF (1988) Weights of evidence modelling: a new approach to mapping mineral potential. Statistical Applications in Earth Sciences 89(9):171–183

Bonham-Carter GF (2002) Geographic information systems for geoscientists: modelling with GIS. In: Merriam, DF (ed). Computer Methods in the Geosciences, 13, Pergamon/Elsevier, New York, pp 302-334

Brabb EE, Harrod BL(eds) (1989) Landslides: Extent and Economic Significance. Balkema Publisher, Rotterdam

Brabb EE (1984) Innovative approaches to landslide hazard and risk mapping. Proceedings of the Fourth International Symposium on Landslides, Canadian Geotechnical Society, Toronto, Canada. 1:307–324

Bui DT, Pradhan B, Lofman O, Revhaug I, Dick OB (2012) Landslide susceptibility assessment in the Hoa Binh province of Vietnam: a comparison of the Levenberg–Marquardt and Bayesian regularized neural networks. Geomorphology 171–172:12–29

Carrara A, Cardinali A, Guzzetti F, Reichenbach P (2001) GIS based techniques for mapping landslide hazard. Research Centre for Informatics and Telecommunication Systems, National Research Council. http://deis158.deis.unibo.it/gis/chapt0.htm(2005-02-15)

Cendrero A, Dramis F (1996) The contribution of landslides to landscape evolution in Europe. Geomorphology 15:191–211

Çevik E, Topal T (2003) GIS-based landslide susceptibility mapping for a problematic segment of the natural gas pipeline, Hendek (Turkey). Environmental Geology 44(8):949–962

Dahal RK, Hasegawa S, Nonomura A, Yamanaka M, Dhakal S, Paudyal P (2008a) Predictive modelling of rainfall-induced landslide hazard in the Lesser Himalaya of Nepal based on weights-of-evidence. Geomorphology 102:496–510

Dahal RK, Hasegawa S, Nonomura A, Yamanaka M, Masuda T, Nishino K (2008b) GIS-based weights-of-evidence modelling of rainfall-induced landslides in small catchments for landslide susceptibility mapping. Environmental Geology 54:311–324

Dai FC, Lee CF, Xu ZW (2001) Assessment of landslide susceptibility on the natural terrain of Lantau Island, Hong Kong. Environmental Geology 40(3):381–391

Dikau R (1989) The application of a digital relief model to landform analysis in geomorphology. In: Raper, J. (ed). Three Dimensional Applications in Geographic Informations Systems. Taylor and Francis, London, pp 51–77

Eidenshink JC (1992) The 1990 conterminous U.S. AVHRR data set. Photogramm. Eng. Remote Sens. 58(6):809-813

Glade T, Anderson M, Crozier MJ (eds) (2005) Landslide hazard and risk. Wiley, NewYork.

Guzzetti P, Reichenbach M, Cardinali M, Galli F, Ardizzone F (2005) Landslide hazard assessment in the Staffora basin, northern Italian Apennines. Geomorphology 72:272–299

Guzzetti F, Carrara A, Cardinali M, Reichenbach P (1999) Landslide hazard evaluation: an aid to a sustainable development. Geomorphology 31:181–216

Guillard C, Zezere J (2012) Landslide susceptibility assessment and validation in the framework of municipal planning in portugal: the case of Loures Municipality. Environmental Management 50:721–735

Kanungo DP, Arora MK, Sarkar, S, Gupta RP (2006) A comparative study of conventional, ANN black box, fuzzy and combined neural and fuzzy weighting procedures for landslide susceptibility zonation in Darjeeling Himalayas. Engineering Geology 85:347–366

Lee CT, Huang CC, Lee JF, Pan KL, Lin ML, Dong JJ (2008) Statistical approach to storm event-induced landslides susceptibility. Natural Hazards and Earth System Sciences 8:941-960

Lee S, Choi J (2004) Landslide susceptibility mapping using GIS and the weight-of-evidence model. International Journal of Geographical Information Science 18:789–814

Lee S, Pradhan B (2007) Landslide hazard mapping at Selangor, Malaysia using frequency ratio and logistic regression models. Landslides 4:33–41

Lee S, Talib JA (2005) Probabilistic landslide susceptibility and factor effect analysis. Environmental Geology 47(7):982-990

Lin CW, Shieh CJ, Yuan BD, Shieh YC, Huang ML, Lee SY (2004) Impact of Chi-Chi earthquake on the occurrence of landslides and debris flows: example from the Chenyulan River watershed, Nantou, Taiwan. Engineering Geology 71:49–61

Lin CW, Liu SH, Lee SY, Liu CC (2006) Impacts of the Chi-Chi earthquake on subsequent rainfall-induced landslides in central Taiwan. Engineering Geology 86:87-101

Lin CW, Chang WS, Liu SH, Tsai TT, Lee SP, Tsang YC, Shieh CL, Tseng CM (2011) Landslides Triggered by the 7 August 2009 Typhoon Morakot in Southern Taiwan. Engineering Geology 123:3–12

Lin CW, Tseng CM, Tseng YH, Fei LY, Hsieh YC, Tarolli P (2013) Recognition of large scale deep-seated landslides in forest areas of Taiwan using high resolution topography. Journal of Asian Earth Sciences 62:389-400

Liu CC, Liu JG, Lin CW, Wu AM, Liu SH, Shieh CL (2007) Image processing of FORMOSAT-2 data for

monitoring South Asia tsunami. International Journal of Remote Sensing 28:3093-3111

Mathew J, Jha VK, Rawat GS (2007) Application of binary logistic regression analysis and its validation for landslide susceptibility mapping in part of Garhwal Himalaya, India. International Journal of Remote Sensing 28(10):2257–2275

Mohammady M, Pourghasemi HR, Pradhan B (2012) Landslide susceptibility mapping at Golestan Province, Iran: a comparison between frequency ratio, Dempster–Shafer,and weights-of-evidence models. Journal of Asian Earth Sciences 61:221–236

Nandi A, Shakoor A (2009) A GIS-based landslide susceptibility evaluation using bivariate and multivariate statistical analyses. Engineering Geology 110:11–20

Neuhäuser B, Terhorst B (2007) Landslide susceptibility assessment using weights-of-evidence applied to a study area at the Jurassic escarpment (SW Germany). Geomorphology 86:12–24

Ozdemir A (2011) Landslide susceptibility mapping using Bayesian approach in the Sultan Mountains (Aks_ehir, Turkey). Natural Hazards 59(3):1573-1607

Ozdemir A, Altural T (2013) A comparative study of frequency ratio, weights of evidence and logistic regression methods for landslide susceptibility mapping: Sultan Mountains, SW Turkey. Journal of Asian Earth Sciences 64:180-197

Pachauri AK, Gupta PV, Chander R (1998) Landslide zoning in a part of the Garhwal Himalayas. Environmental Geology 36:325–334

Papoulis A. (1984). Probability, Random Variables, and Stochastic Processes, 2nd edition. Section 7.3. New York: McGraw-Hill.

Piacentini D, Troiani F, Soldati M, Notarnicola C, Savelli D, Schneiderbauer S, Strada C (2012) Statistical analysis for assessing shallow-landslide susceptibility in South Tyrol (south-eastern Alps, Italy). Geomorphology 151-152:196-206

Poudyal CP, Chang C, Oh HJ, Lee S (2010) Landslide susceptibility maps comparing frequency ratio and artificial neural networks: a case study from the Nepal Himalaya. Environmental Earth Sciences 61:1049–1064

Poli S, Sterlacchini S (2007) Landslide representation strategies in susceptibility studies using weights-of-evidence modeling technique. Natural Resources Research 16:121–134

Pradhan B, Lee S (2010a) Delineation of landslide hazard areas on Penang Island, Malaysia, by using frequency ratio, logistic regression, and artificial neural network models. Environmental Earth Sciences 60:1037–1054

Pradhan B, Lee S (2010b) Regional landslide susceptibility analysis using back-propagation neural network model at Cameron Highland, Malaysia. Landslides 7(1):13–30

Pradhan B, Lee S (2010c) Landslide susceptibility assessment and factor effect analysis: back-propagation artificial neural networks and their comparison with frequency ratio and bivariate logistic regression modelling. Environmental Modelling & Software 25:747–759

Pradhan B (2011) Manifestation of an advanced fuzzy logic model coupled with Geo-information techniques to landslide susceptibility mapping and their comparison with logistic regression modelling. Environmental and Ecological Statistics 18:471-493

524 Regmi NR, Giardino JR, Vitek JD (2010) Modeling susceptibility to landslides using the weight of evidence
525 approach: Western Colorado, USA. Geomorphology 115:172–187
526 Saha AK, Gupta RP, Arora MK (2002) GIS-based landslide hazard zonation in the Bhagirathi(Ganga) valley,
527 Himalayas. International Journal of Remote Sensing 23(2):357–369
528 Schicker R, Moon V (2012) Comparison of bivariate and multivariate statistical approaches in landslide
529 susceptibility mapping at a regional scale. Geomorphology 162:40–57
530 Shahabi H, Khezri S, Ahmad BB, Hashim M (2014) Landslide susceptibility mapping at central Zab basin,
531 Iran: A comparison between analytical hierarchy process, frequency ratio and logistic regression models.
532 Catena 115:55-70
533 Tang C, Zhu J, Qi X, Ding J (2011) Landslides induced by the Wenchuan earthquake and the subsequent
534 strong rainfall event: A case study in the Beichuan area of China. Engineering Geology 122:22-33
535 Tsou CY, Feng ZY, Chigira M (2011) Catastrophic landslide induced by Typhoon Morakot, Shiaolin,
536 Taiwan. Geomorphology 127:166–178
537 Tseng CM, Lin CW, Stark CP, Liu JK, Fei LY, Hsieh YC (2013) Application of a Multi-temporal,
538 LiDAR-derived, Digital Terrain Model in a Landslide-Volume Estimation. Earth Surface Processes and
539 Landforms 38:1587-1601
540 Van Westen CJ, Castellanos E, Kuriakose SL (2008) Spatial data for landslide susceptibility, hazard, and
541 vulnerability assessment: an overview. Engineering Geology 102(3-4):112–131
542 Van Westen CJ, Rengers N, Soeters R (2003) Use of geomorphological information in indirect landslide
543 assessment. Natural Hazards 30:399–419
544 Vijith H, Madhu G (2008) Estimating potential landslide sites of an upland sub-watershed in Western Ghat's
545 of Kerala (India) through frequency ratio and GIS. Environmental Geology 55:1397–1405
546 Wilson JP, Gallant JG (2000) Terrain analysis principles and applications. John Wiley and Sons, Inc.,
547 New-York.
548 Xu C, Xu X, Dai F, Xiao J, Tan X, Yuan R (2012) Landslide hazard mapping using GIS and weight of
549 evidence model in Qingshui River watershed of 2008 Wenchuan earthquake struck region. Journal of
550 Earth Science 23:97–120
551 Yalcin A (2008) GIS-based landslide susceptibility mapping using analytical hierarchy process and bivariate
552 statistics in Ardesen (Turkey): comparisons of results and confirmations. Catena 72(1):1–12
553 Yalcin A, Reis S, Aydinoglu AC, Yomralioglu T (2011) A GIS-based comparative study of frequency ratio,
554 analytical hierarchy process, bivariate statistics and logistics regression methods for landslide
555 susceptibility mapping in Trabzon, NE Turkey. Catena 85:274–287
556 Yilmaz I (2009) Landslide susceptibility mapping using frequency ratio, logistic regression, artificial neural
557 networks and their comparison: a case study from Kat landslides (Tokat-Turkey). Computers &
558 Geosciences 35:1125–1138
559 Yilmaz I (2010a) Comparison of landslide susceptibility mapping methodologies for Koyulhisar, Turkey:
560 conditional probability, logistic regression, artificial neural networks, and support vector machine.
561 Environmental Earth Sciences 61:821–836
562 Yilmaz I (2010b) The effect of the sampling strategies on the landslide susceptibility mapping by conditional

probability and artificial neural networks. Environmental Earth Sciences 60(3):505–519

Table 1 FORMOSAT-2 images used to map the event-based landslide inventories in this study

Typhoon event	Date	Date of images taken (pre//post of typhoon)
Mitag	2007/11/26 ~ 11/27	2007/10/26, 2007/11/20 // 2007/12/21, 2008/02/17
Kalmaegi	2008/07/16 ~ 07/18	2007/12/21, 2008/02/17 // 2008/07/23, 2008/08/24
Sinlaku	2008/09/11 ~ 09/16	2008/07/23, 2008/08/24 // 2008/12/21, 2009/01/14
Morakot	2009/08/05 ~ 08/10	2008/12/21, 2009/01/14 // 2009/08/17, 2009/08/21

Table 2 Landslide data interpreted from FORMOSAT-2 images for the four typhoon events

Typhoon event	Rainfall statistics (mm)				Landslide area (ha)	Landslide ratio (%)
	Max.	Min.	Mean.	S.D.		
Mitag	225	10	60	38	440	0.322
Kalmaegi	993	208	712	168	1452	1.062
Sinlaku	1251	194	774	223	593	0.434
Morakot	3394	906	2323	445	8946	6.544

Table 3 Test results for various combinations of dominant factors of landslides

(a) Typhoon Mitag and Sinlaku

No.	Combination of factors	Training AUC	
		Mitag	Sinlaku
A1	Sa+Lc	0.561	0.606
A2	Sa+Lc+As	0.708	0.786
A3	Sa+Lc+Lf	0.567	0.618
A4	Sa+Lc+El	0.682	0.697
A5	Sa+Lc+Dl	0.596	0.633
A6	Sa+Lc+Ds	0.634	0.681
A7	Sa+Lc+Nv	0.799	0.857
A8	Sa+Lc+Nv+As	0.870	0.912
A9	Sa+Lc+Nv+Lf	0.801	0.859
A10	Sa+Lc+Nv+El	0.824	0.891
A11	Sa+Lc+Nv+Dl	0.810	0.865
A12	Sa+Lc+Nv+Ds	0.817	0.872
A13	Sa+Lc+Nv+As+Lf	0.870	0.913
A14	Sa+Lc+Nv+As+El	0.882	0.931
A15	Sa+Lc+Nv+As+Dl	0.874	0.915
A16	Sa+Lc+Nv+As+Ds	0.879	0.920
A17	Total eight factors	0.888	0.933

Sa: Slope angle; Lc: Lithology condition; As: Aspect; Lf: Landform; El: Elevation; Dl: Distance to lineation; Ds: Distance to stream; Nv: NDVI.

601
602 (b) Typhoon Kalmaegi

No.	Combination of factors	Training AUC
		Kalmaegi
B1	Sa+Lc	0.616
B2	Sa+Lc+As	0.626
B3	Sa+Lc+Lf	0.628
B4	Sa+Lc+El	0.643
B5	Sa+Lc+Dl	0.624
B6	Sa+Lc+Ds	0.649
B7	Sa+Lc+Nv	0.820
B8	Sa+Lc+Nv+As	0.791
B9	Sa+Lc+Nv+Lf	0.823
B10	Sa+Lc+Nv+El	0.823
B11	Sa+Lc+Nv+Dl	0.821
B12	Sa+Lc+Nv+Ds	0.826
B13	Sa+Lc+Nv+Ds+As	0.815
B14	Sa+Lc+Nv+Ds+Lf	0.829
B15	Sa+Lc+Nv+Ds+El	0.831
B16	Sa+Lc+Nv+Ds+Dl	0.828
B17	Total eight factors	0.824

603
604
605 (c) Typhoon Morakot

No.	Combination of factors	Training AUC
		Morakot
C1	Sa+Lc	0.556
C2	Sa+Lc+As	0.579
C3	Sa+Lc+Lf	0.568
C4	Sa+Lc+Nv	0.576
C5	Sa+Lc+Dl	0.568
C6	Sa+Lc+Ds	0.582
C7	Sa+Lc+El	0.624
C8	Sa+Lc+El+As	0.635
C9	Sa+Lc+El+Lf	0.626
C10	Sa+Lc+El+Dl	0.626
C11	Sa+Lc+El+Ds	0.633
C12	Sa+Lc+El+Nv	0.636
C13	Sa+Lc+El+Nv+As	0.646
C14	Sa+Lc+El+Nv+Lf	0.639
C15	Sa+Lc+El+Nv+Dl	0.637
C16	Sa+Lc+El+Nv+Ds	0.642
C17	Total eight factors	0.657

606
607

608
609 **Table 4** Validation results of landslide susceptibility model developed by each typhoon

Events	LR (%)	AUC (Training)	AUC (Validation)			
			Mitag	Kalmaegi	Sinlaku	Morakot
Mitag	0.322	0.888		0.796	0.889	0.603
Kalmaegi	1.062	0.824	0.712		0.636	0.512
Sinlaku	0.434	0.933	0.902	0.844		0.648
Morakot	6.544	0.657	0.656	0.582	0.737	

610
611
612
613
614
615 **Table 5** Distribution of landslides induced by the four typhoons for each susceptibility
616 level

Typhoon events	Very high (0~10%)	High (10%~30%)	Moderate (30%~50%)	Low (50%~70%)	Very low (70%~100%)
Mitag	73.47%	18.98%	4.26%	2.33%	0.96%
Kalmaegi	50.04%	33.11%	12.09%	4.34%	0.42%
Sinlaku	80.49%	15.61%	3.13%	0.57%	0.21%
Morakot	19.38%	30.50%	22.17%	14.71%	13.24%

617
618
619
620
621 **Table 6** Comparison of the WOE model performance in different literatures

Source	Evaluated area (km^2)	Model performance (%)
Neuhäuser and Terhorst (2007)	500	95
Dahal et al. (2008a)	18.9	85.5
Dahal et al. (2008b)	4	80.7
Regmi et al. (2010)	815	78
Mohammady et al. (2012)	12050	69
Piacentini et al. (2012)	7500	75
Ozdemir and Altural (2013)	373	73.6
This study	1367	90.2

622
623

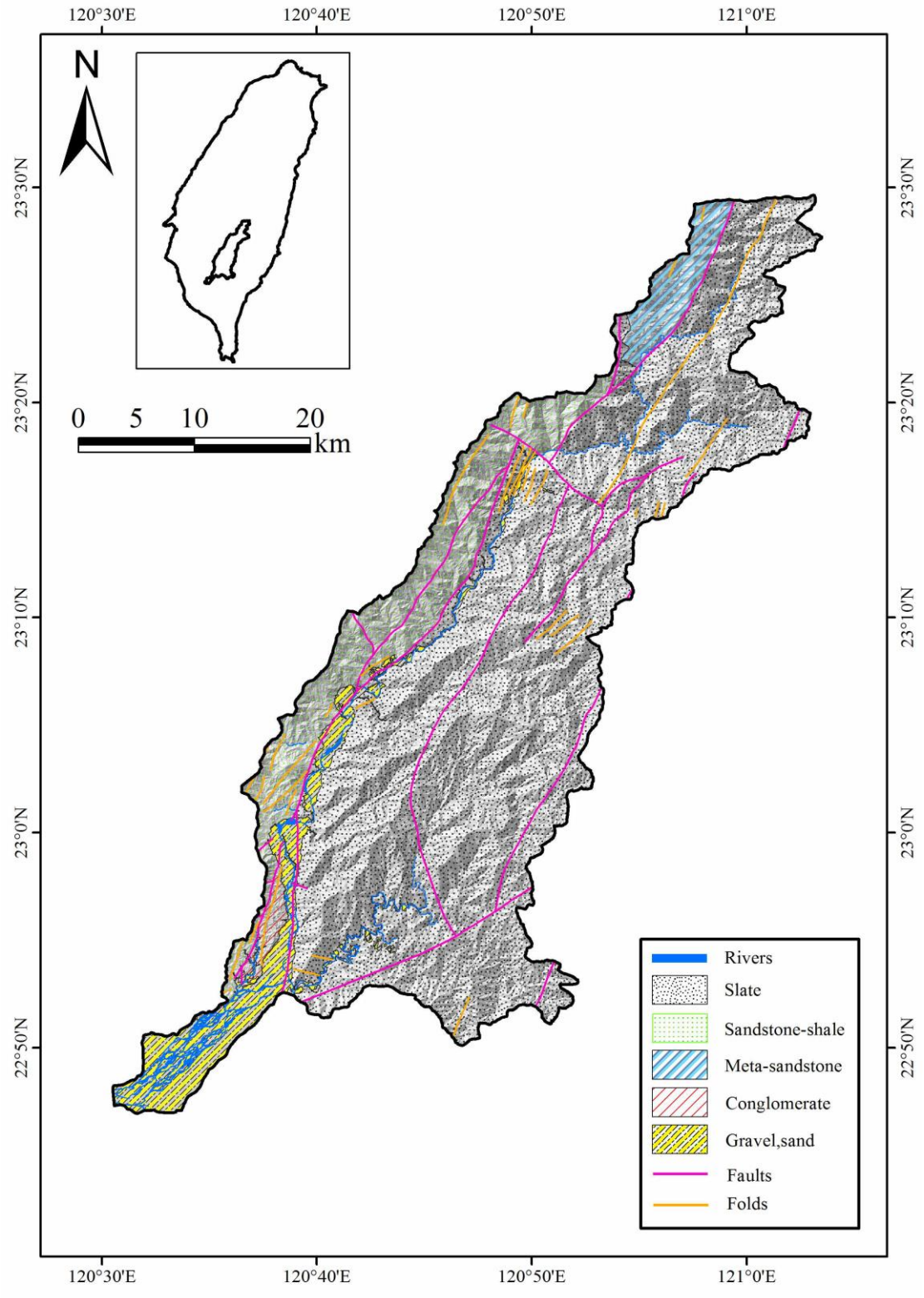

Fig. 1 Geological map of the study area. The bold black line shows the study area.

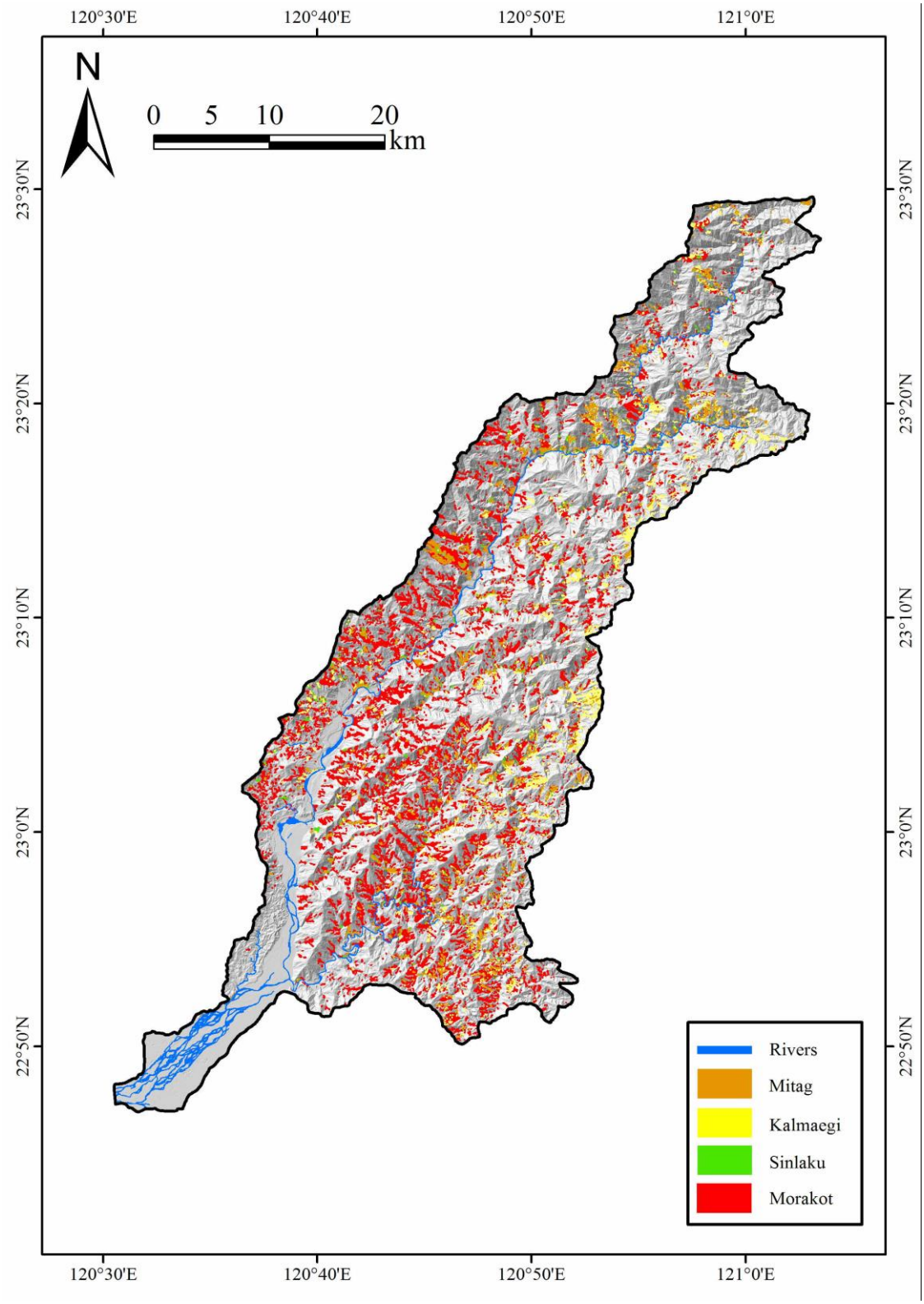

Fig. 2 Event-based landslide inventories interpreted by multi-temporal FORMOSAT-2 satellite images.

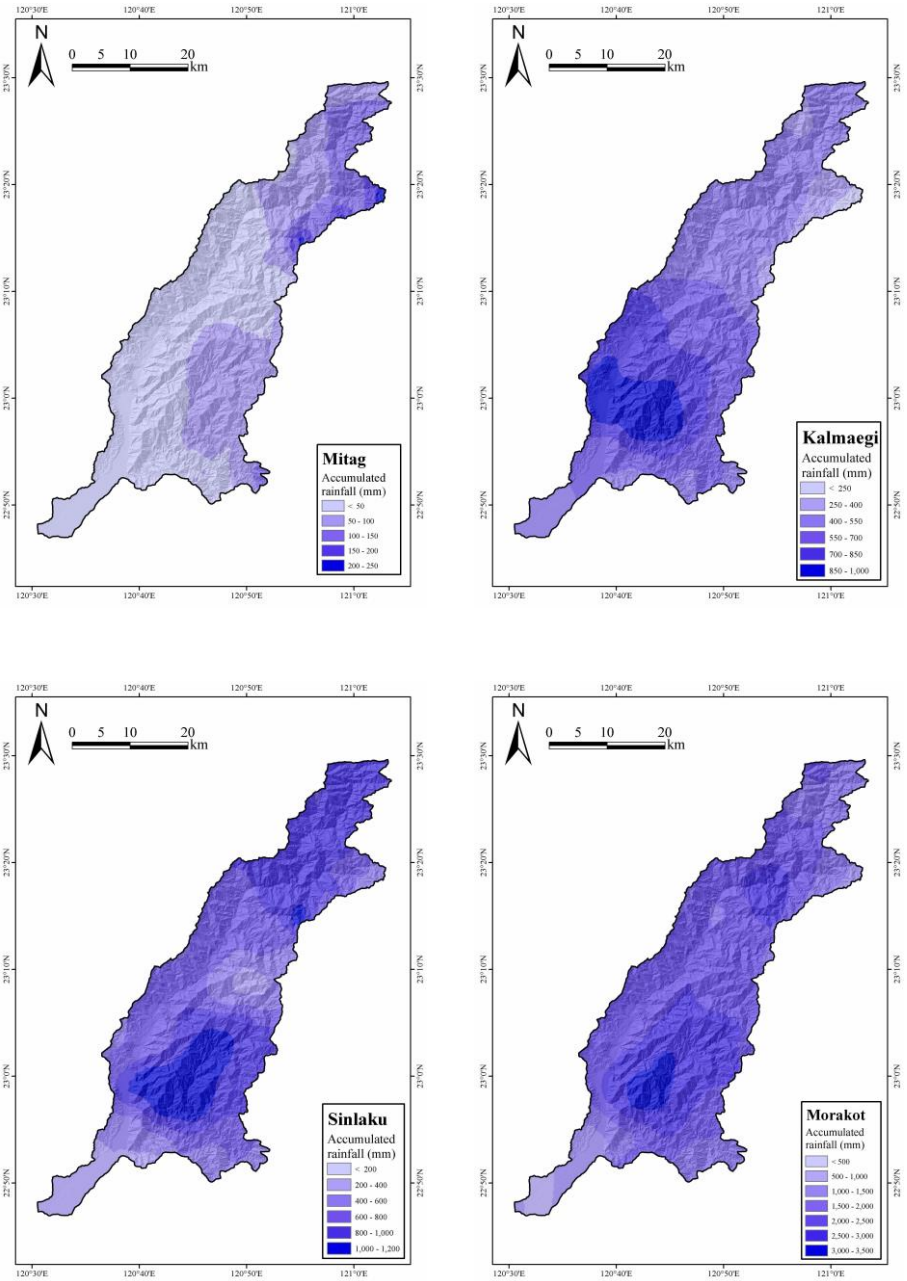

Fig. 3 Spatial distribution of accumulated rainfall of four typhoon events

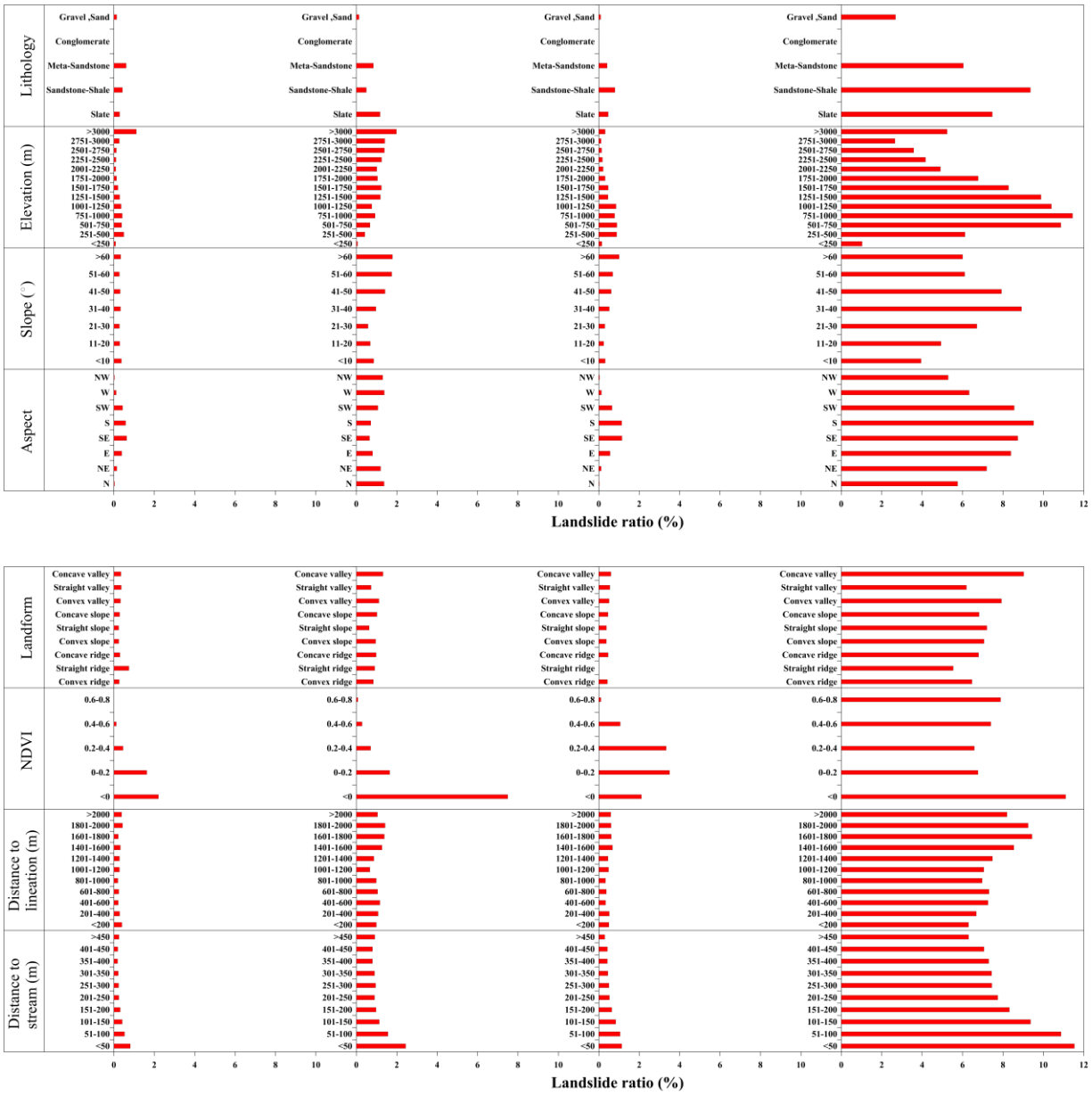

(a) Typhoon Mitag (b) Typhoon Kalmaegi (c) Typhoon Sinlaku (d) Typhoon Morakot

Fig. 4 Landslide ratios for the eight landslide affecting factors of the four typhoon events.

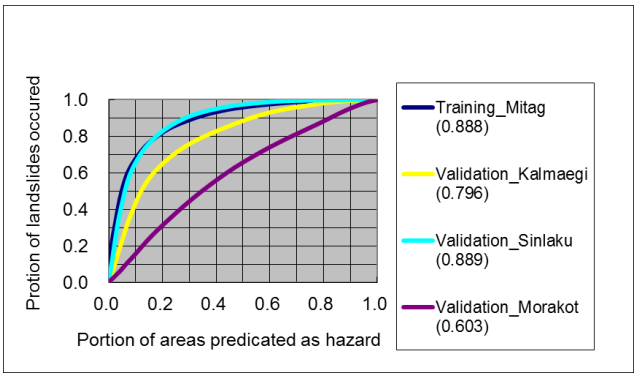

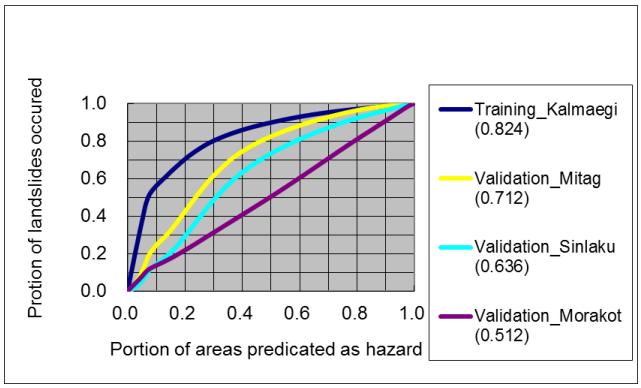

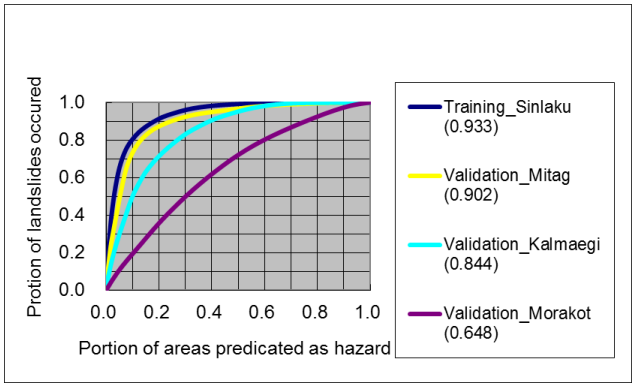

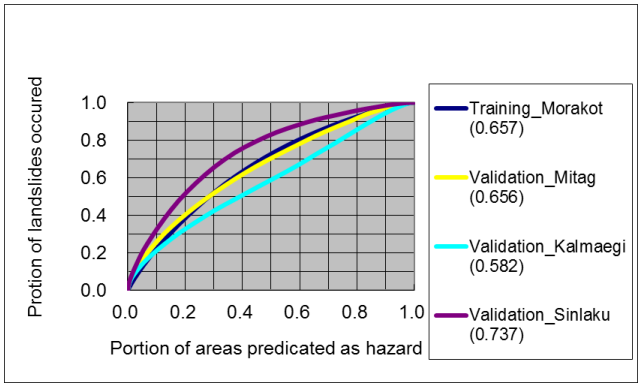

Fig. 5 The training and validation curves of four typhoon events

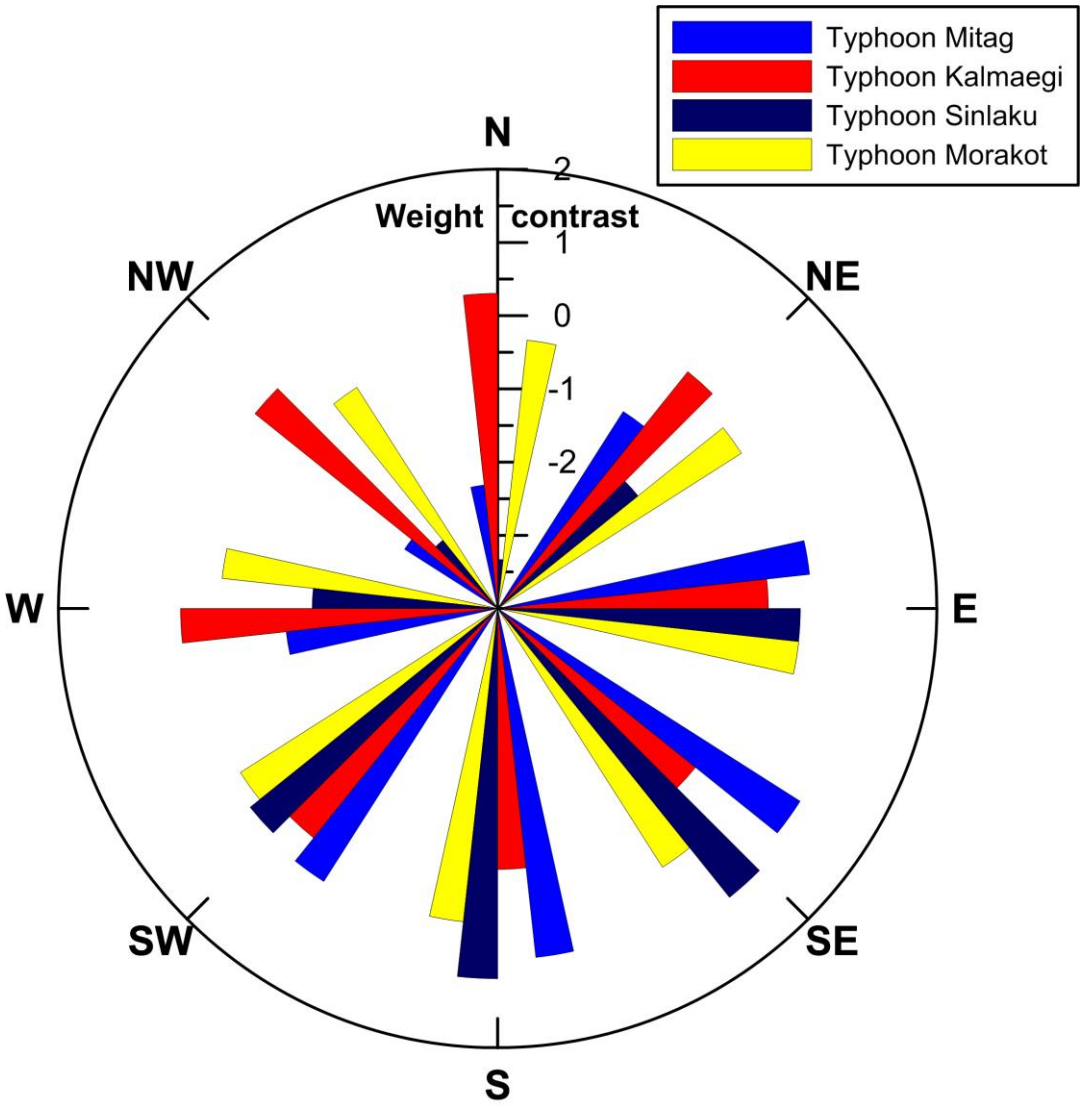

Fig. 6 Variation of weight contrast at different slope aspect directions.

671

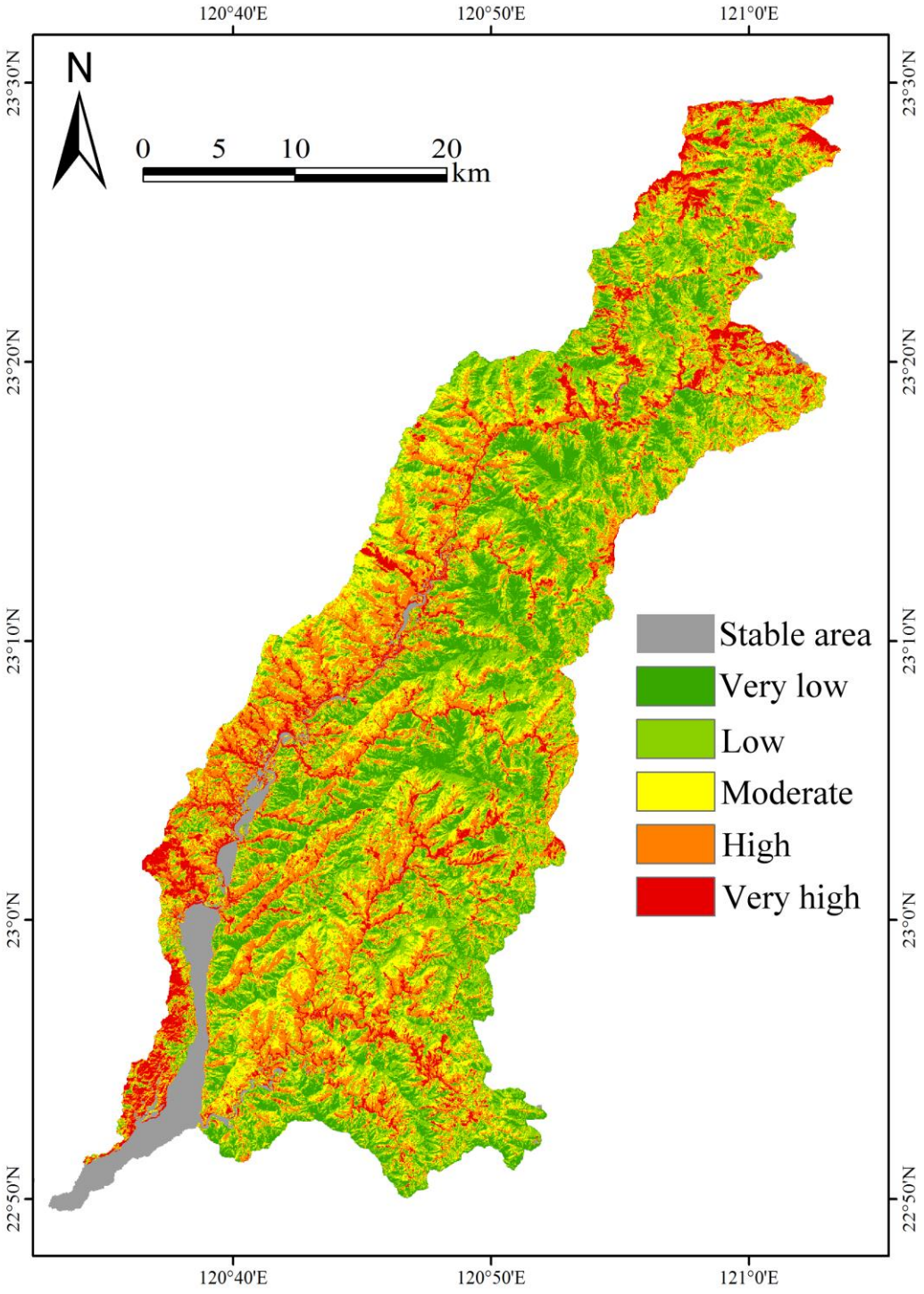

672
673
674 **Fig. 7** Landslide susceptibility map of the study area.
675